Energy 72 (2014) 242–253

Contents lists available at ScienceDirect

Energy

journal homepage: www.elsevier.com/locate/energy

Combustion of $CH_4/O_2/N_2$ in a well stirred reactor

Feifei Wang [a], Pengfei Li [a], Zhenfeng Mei [a], Jianpeng Zhang [a], Jianchun Mi [a, b, *]

[a] State Key Laboratory of Turbulence and Complex Systems, College of Engineering, Peking University, Beijing 100871, China
[b] College of Energy & Power Engineering, Changsha University of Science and Technology, Changsha 410004, China

ARTICLE INFO

Article history:
Received 21 November 2013
Received in revised form
4 May 2014
Accepted 10 May 2014
Available online 6 June 2014

Keywords:
Well stirred reactor (WSR)
Self-ignition
Extinction
Moderate and intense low-oxygen dilution (MILD) combustion

ABSTRACT

Detailed kinetic calculations of chemical reactions using GRI-Mech 3.0 are carried out to characterize the combustion of $CH_4/O_2/N_2$ mixture in a well-stirred reactor (WSR). Very wide ranges of the inlet temperature T_{in} (300 K–2700 K), nitrogen dilution concentration (0%–99%) and global equivalence ratio (0.5–4.0) are considered. The extinction and self-ignition temperatures (T_{ex} and T_{si}) of the $CH_4/O_2/N_2$ mixture are identified by the ignition-extinction *S*-curve. Based on T_{ex}, T_{si} T_{WSR}, and the operative conditions (T_{in} and the mixture composition), the WSR combustion of $CH_4/O_2/N_2$ can be quantitatively classified into several particular regimes. Moreover, the product composition and elementary chemical pathways of the CH_4 oxidation are also examined. Results demonstrate that the WSR working temperature determines the chemical characteristics of the CH_4 oxidation rather than the combustion regime.

1. Introduction

The moderate and intense low-oxygen dilution (MILD) combustion, termed formally by Cavaliere and de Joannon [1], is one of the newly developing combustion technologies. This combustion is similar, but not identical (see below), to those that debuted a few years earlier, i.e., the flameless oxidation (FLOX) [2] and the high temperature air combustion (HiTAC) [3,4]. So far, significant benefits of these technologies for industrial applications have been well demonstrated, e.g., producing efficient combustion [4,5] and in particular extremely low NO_x emissions [6,7]. These technologies are commonly featured by highly distributed reaction zone [8], uniform thermal field [9], and low luminescence [4,10]. Accordingly, in recent years the HiTAC and FLOX are often treated identical to the "MILD combustion". Note, however, that those technologies are not exactly identical, as indicated by Cavaliere and de Joannon [1] and further argued below.

Wünning and Wünning [2] carried out a series of experiments on diffusion combustion of burning methane (CH_4) using a flameless oxidation (FLOX) burner. Based on the data obtained, they delivered a mapping of different combustion regimes. As reproduced in Fig. 1(a), three combustion regimes are evident: (i) traditional combustion (TC) occurring possibly over the entire range of the furnace temperature but only for the dimensionless recirculation rate $K_v \leq 0.3$ (somewhat increased at higher temperatures); (ii) flameless oxidation (FLOX), i.e., combustion reactions occurring invisibly in a highly stable form when both the furnace temperature is well beyond the self-ignition temperature of the mixture (T_{si}) and the entrained flue gas recirculation rate $K_v \geq 3$; (iii) unstable combustion (UC) for $3 > K_v > 0.3$, which intermittently switches between TC and FLOX. Within the UC regime, the flame may lift off and finally extinct for temperatures $< T_{si}$.

Nippon Furnace Kogyo Kaisha Company [3] meanwhile, taking a different route, developed a new combustion process by preheating the combustion air to a temperature $T_{air} > T_{si}$, usually around 1200 K. Katsuki and Hasegawa [3] termed it as the high temperature air combustion (HiTAC), where the "high temperature" means that $T_{air} > T_{si}$. Namely, HiTAC is somewhat different from the FLOX, see Fig. 1(a, b). Tsuji et al. [4] considered the traditional preheated air combustion (PAC) as the one with $T_{air} < T_{si}$. Fig. 1(b) shows the auto-ignition and forced-ignition limits, derived from the oxygen concentration and air temperature (two external injection parameters), for propane (C3H8) jet in hot air diluted with nitrogen, from which two combustion regimes, i.e., PAC and HiTAC, are defined. Comparison of Fig. 1(a) and (b) reveals that the traditional and unstable combustion (TC and UC) at $T_{air} > T_{si}$ and FLOX of Wünning and Wünning [2] altogether are equivalent to the HiTAC of Katsuki and Hasegawa [3]. In other words, FLOX is only a subset of HiTAC, and hence the two are not identical. Unfortunately, the border of FLOX cannot be determined from refs. 1, 3, and 4.

* Corresponding author. J. Mi, at State Key Laboratory of Turbulence and Complex Systems, College of Engineering, Peking University, Beijing 100871, China. Tel.: +86 010 62767074.
E-mail address: jcmi@coe.pku.edu.cn (J. Mi).

http://dx.doi.org/10.1016/j.energy.2014.05.029
0360-5442/

Cavaliere and de Joannon [1] analyzed the FLOX and HiTAC and concluded that those technologies or the like all use moderate or intense low-oxygen dilution, which can be abridged as 'MILD'. These authors defined the 'MILD combustion' in a rigorous and quantitative fashion. That is, the occurrence of MILD combustion requires: (1) the inlet temperature of the reactant mixture $T_{in} > T_{si}$, and (2) the allowable maximum temperature rise due to combustion $\Delta T < T_{si}$. Based on these conditions, they drew a very simple T_{in}–ΔT diagram that unambiguously shows different combustion regimes of burning $CH_4/O_2/N_2$ in a WSR, see Fig. 1(c), with a 1.0 s residence time and at atmospheric pressure; they termed these regimes as the feedback combustion (FC), high temperature combustion (HTC) and moderate or intense low-oxygen dilution (MILD) combustion. From Refs. [1,3], both MILD and HTC regimes are subsets of HiTAC of Katsuki and Hasegawa [3] while FC is somehow identical to PAC.

Following Cavaliere and de Joannon [1], the classification of the above similar technologies, i.e., FLOX, HiTAC and MILD combustion, has been extensively investigated using the counter-flow configurations [11–14]. In those studies, different combustion regimes of the diffusion flames had been well achieved and evaluated under various non-premixed combinations of hot and diluted fuel/oxidant flow, e.g., hot oxidant and diluted fuel (HODF) [11,12], hot fuel and diluted fuel (HFDF) [13], and also hot oxidant and diluted oxidant (HODO) [14]. Note that all those previous studies cited [1–14] on the FLOX, HiTAC or MILD combustion were performed for the highly-diluted low-oxygen cases. However, we have found that the quantitative mathematical conditions of $T_{in} > T_{si}$ and $\Delta T < T_{si}$ for MILD combustion, which were derived by Cavaliere and de Joannon [1], do not require reactants to be highly diluted. Based on this finding, our recent work [15] has been conducted to investigate the combustion regime for fuel-jet flames in hot co-flow (JHC) with the oxygen concentration X_{O2} = 0%–100% and temperature T_{cof} = 200 K–2400 K. We found that the JHC flames can be also classified into three regimes: traditional combustion (TC), high temperature combustion (HTC), and flameless combustion (FLC). The FLC regime can be further divided into three distinct sub-zones, i.e., MILD, MILD-like and Quasi-MILD. Here, the MILD and MILD-like combustion both satisfy the MILD conditions ($T_{cof} > T_{si}$ and $\Delta T < T_{si}$) of Cavaliere and de Joannon [1] while the quasi-MILD combustion does not. Moreover, the MILD-like combustion occur in the non-diluted and enriched cases where $X_{O2} > 21\%$ for the sufficiently high co-flow temperature. Apparently, the MILD-like combustion has broken the 'prerequisite' of low-oxygen for the occurrence of MILD combustion. Nevertheless, it is not clear that whether this recent finding [15] is still appropriate to describe the combustion regimes in a well-stirred reactor (WSR).

On the other hand, de Joannon et al. [16,17] conducted the analysis of methane oxidation in a well-stirred reactor (WSR) to evaluate the diluted MILD combustion. They found that the overall reaction mechanism of CH_4 oxidation varies with different WSR working temperature (T_{WSR}) [16]. It was also found that the competition between the exoergic oxidation and the endothermic recombination plays an important role under MILD condition [17]. As T_{WSR} is increased to 1200 K, the $C_{(2)}$ compounds become prevalent and the endothermic recombination is favored over the oxidative one. However, the previous studies [16,17] were carried out only for the diluted case, leaving the non-diluted and enriched cases of combustion open for further investigations.

Moreover, elementary chemical pathways of fuel oxidation differ greatly under various reacting temperatures [18]. The variation of the combustion regime may result in different reacting temperature and then causes the pathway change of the fuel oxidation. From this point, Plessing et al. [8] carried out the instantaneous measurements of temperature and OH concentration in a recuperative furnace. They found that, under MILD condition, OH is homogeneously distributed to a relatively larger region and its concentration in the combustion zone is lower than that under traditional combustion condition. Compared with the traditional combustion, the intermediate products such as OH and CO were found to be extremely suppressed when operating at MILD condition, which has also reported by Dally et al. [19]. Using a fuel jet in hot low-oxygen coflow (JHC) device, Dally et al. [19] emulated the MILD combustion and deduced that there would be difference of the chemical pathways between the highly-diluted and non-diluted JHC flames. To date, however, although abundant previous studies cited [1–17] have been performed on the MILD combustion, little attention has been paid on the comparison of reaction pathways of fuel oxidation under different combustion regimes.

Accordingly, to fill the gaps noted above, the present study is designated to characterize the WSR combustion of diluted, non-diluted and enriched CH_4/O_2 mixture. Based on the ignition-extinction *S*-curve, the extinction and self-ignition temperatures (T_{ex} and T_{si}) of the $CH_4/O_2/N_2$ mixture at different compositions are systematically investigated. The main objectives of this study are twofold:

(i) To quantitatively classify the combustion regimes in a WSR over the full range of oxygen (0%–100%) that extends the previous understanding of MILD combustion derived from Cavaliere and de Joannon [1]; and
(ii) To examine the overall and elementary chemical pathways of CH_4 oxidation occurring under different WSR combustion regimes.

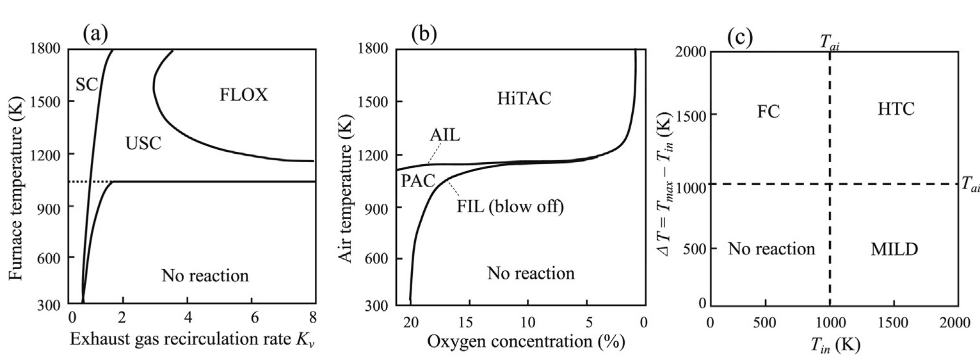

Fig. 1. Different combustion regimes. (a) Stability limits of firing CH_4/air, based on the in-furnace or internal parameters [2], where FLOX = Flameless Oxidation, TC = Traditional Combustion, and UC = Unstable Combustion; (b) auto-ignition limit (AIL) and forced-ignition limit (FIL) of C_3H_8 in preheated air or diluted air with N_2, based on the external parameters [3,4]; (c) $T_{in} - \Delta T$ locus of different WSR combustion regimes for a mixture of $CH_4/O_2/N_2$ at atmospheric pressure and a residence time of 1 s, where FC = Feedback Combustion, HTC = High Temperature Combustion and MILD = Moderate or Intense Low-oxygen Dilution [1].

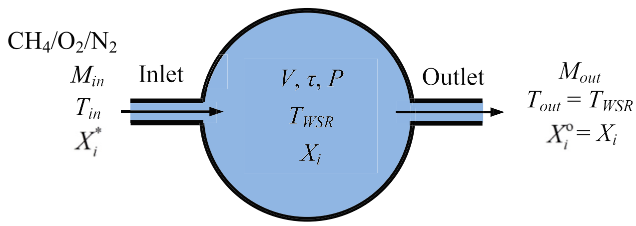

Fig. 2. Schematic diagram of the well stirred reactor (WSR).

2. Computational approach

Present numerical simulations of the premixed $CH_4/O_2/N_2$ combustion in a WSR are performed using CHEMKIN 4.1 [20] software. The reactor is an ideal model, where reactants can be mixed perfectly before reactions take place. This model has been used to study many aspects of combustion such as flame stabilization and NO_x formation. The reactions in the WSR take place in a homogeneous and adiabatic environment and may be approximated to those locally occurring at a spatial point in practical furnaces. Therefore, spatial distributions of species usually encountered in industrial combustors are not considered in WSR. Fig. 2 shows a schematic diagram of the present WSR model. On the diagram, V, P and τ are the volume, pressure and mixture residence time in the reactor; X_i and T_{WSR} are the mole fraction of species i and the mixture temperature in the reactor; X_i^* and T_{in} denote the mole fraction of inlet species i and the inlet mixture temperature; X_i^o and T_{out} indicate the mole fraction of outlet species i and the outlet mixture temperature. In this study, V and P are taken to be 67.4 cm^3 and 1.0 atm. The residence time τ can be used as a characteristic parameter of the reactor. The system is assumed adiabatic and so the heat exchange between the reactor and the ambient is set zero. The total mass flow rate (M_{in}) into the reactor is equal to that (M_{out}) issuing out from the reactor without any mass exchange with the surrounding. The mass flow rate $M_{in} = M_{out}$ is related to V and τ by $M_{in} = \rho V/\tau$, where ρ is the density of the gas mixture inside the reactor. To summarize, the perfectly premixed $CH_4/O_2/N_2$ mixture at T_{in} flows into the reactor, CH_4 reacts with O_2 when T_{in} is sufficiently high and then the combustion products flow out from the reactor. The mixture residence time τ can be varied by changing the mixture mass flow rate M_{in} or the reactor volume V.

All calculations use the detailed mechanism of GRI-Mech 3.0 [21] which consists of 53 species for a total of 325 reversible reactions. GRI-Mech 3.0 is an optimized mechanism that was designed to model natural gas (mainly CH_4) combustion under the conditions of temperature varying from 1000 K to 2500 K, pressure from 10 Torr to 10 atm, and equivalence ratio from 0.1 to 5.0. Note also that the thermal properties involved in GRI-Mech 3.0 are ranged from 200 K to 3000 K. The previous studies have shown its ability in modeling air-diluted [22], CH_4/air [23], and oxy-enriched diffusion flames [24].

3. Modeling validation

To validate the present modeling, we model the CH_4/air combustion in the WSR under the same conditions as those used in the experiments of Steven and Joseph [25]. The temperature of the inlet CH_4 and air is 298 K. The CH_4/air mixture is burned over the equivalence ratio from 0.53 to 1.63 and the average residence time of the mixture in the reactor is 0.0085 s.

Fig. 3 compares the present calculations with the experimental data and the previous predictions of Steven and Joseph [25]. Obviously, the present WSR and previous numerical results both predict well T_{WSR} and X_{O2} over the broad equivalence ratio range. Consistent with the measurements, the predictions show a slight rise of X_{O2} when $\varphi > 1.4$. Apparently, at the fuel rich conditions of $\varphi > 1.4$, T_{WSR} is relatively low (see Fig. 3(a)) that the oxidation of CH_4 cannot process completely over the residence time. Moreover, although the predictions of X_{CO2} are less satisfactory, their variable trend is similar to the measurement. Accordingly, the present WSR model with GRI-Mech 3.0 is effective in simulating the WSR combustion of CH_4/air and hence can be used in the subsequent sections.

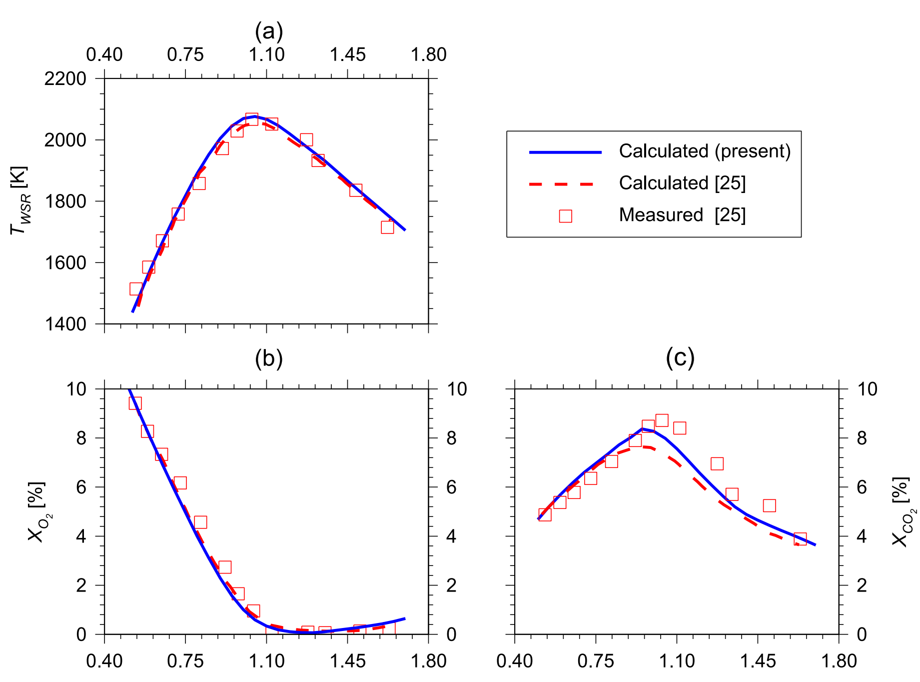

Fig. 3. Comparisons between the predictions and the measurements [25] of (a) T_{WSR}, (b) X_{O2} and (c) X_{CO2}.

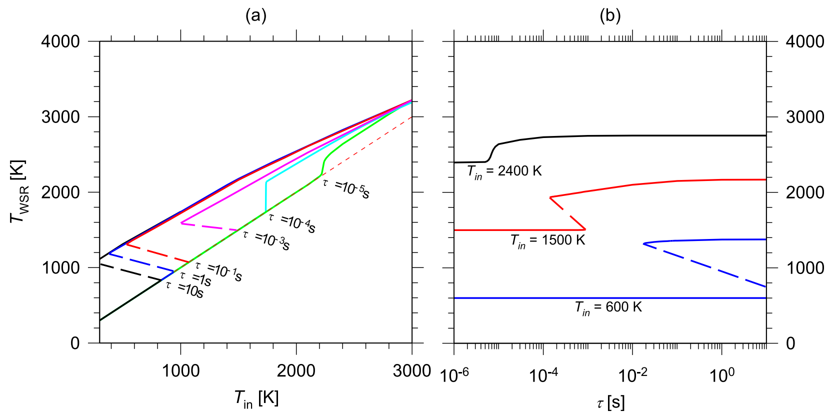

Fig. 4. WSR working temperatures (T_{WSR}) versus (a) the inlet mixture temperature (T_{in}) and (b) the residence time (τ) for the $CH_4/O_2/N_2$ mixture at 6.7% O_2, 3.3% CH_4 and 90% N_2.

4. Ignition and extinction of WSR combustion

Fig. 4 plots T_{WSR} versus T_{in} with T_{in} = 300 K–3000 K and T_{WSR} versus τ with the residence time (10^{-5} s ~ 10 s) for the reactant mixture (6.7% O_2 + 3.3% CH_4 + 90% N_2). In Fig. 4, the well-known ignition-extinction *S*-curves [26] are illustrated. The upper and lower branches of the *S*-curve represent the states of strong burning and weak oxidation whereas the middle branch of the *S*-curve (dashed line) is the unstable state that cannot be obtained experimentally. In Fig. 4(a), $T_{in} = T_{ex}$ at the upper turning point is the maximum temperature of extinction of the strong burning flame, i.e., 'extinction temperature', while $T_{in} = T_{si}$ at the lower turning point is considered as the minimum temperature of reactant self-ignition, often termed as 'self-ignition temperature'. Similarly, in Fig. 4(b), the turning point ($\tau = \tau_{ex}$) of the upper branch is the maximum residence time below which the flame extinction occurs whereas the lower turning point of $\tau = \tau_{si}$ is considered as the minimum residence time of the self-ignition.

In Fig. 4(a), as T_{in} is increased to T_{si}, the mixture reaction occurs spontaneously and T_{WSR} jumps from the lower branch up to the upper branch; then T_{WSR} increases along the upper branch as T_{in} is further increased. Fig. 4(a) also demonstrates that both T_{si} and T_{ex} climb as τ is shortened. This can be easily understood here. A shorter τ causes less heat released in the reactor and hence requires a higher T_{in} for the reaction maintaining. Fig. 4(b) shows that, at T_{in} = 600 K, the WSR mixture may be not ignited by increasing the residence time. In contrast, when T_{in} is escalated, the residence time for the ignition is reduced significantly. This should result from the fact that the increase of T_{in} makes the reactants more active, which hence allows the τ_{ex} and τ_{si} to decrease. In addition, as T_{in} is increased, the difference between T_{si} and T_{ex} narrows and finally disappears.

Moreover, Cavaliere and de Joannon [1] analyzed the different combustion regimes of $CH_4/O_2/N_2$ combustion in a WSR with the residence time τ = 1.0 s and at atmospheric pressure (1 atm). For consistency with their investigation, this study also uses this value of τ for calculations presented hereafter.

Fig. 5 illustrates the T_{WSR} against T_{in} with τ = 1 s for four mixture compositions, i.e., 66.7% O_2 + 33.3% CH_4 (O_2 + CH_4), 19% O_2 + 9.5% CH_4 + 71.5% N_2 (air + CH_4), 6.7% O_2 + 3.3% CH_4 + 90% N_2 (diluted oxidant + CH_4), and 0.67% O_2 + 0.33% CH_4 + 99% N_2 (extremely diluted oxidant + CH_4). Results demonstrate that, as $X^*_{N_2}$ is increased, the middle branch shifts up to higher values of T_{in}, which was also reported in Refs. [1,16]. That is, both T_{si} and T_{ex} increase when adding more N_2 into the reactant mixture. Moreover, similar to its dependence on T_{in} and τ (Fig. 4), the difference between T_{si} and T_{ex} narrows with increasing $X^*_{N_2}$ and nearly vanishes at

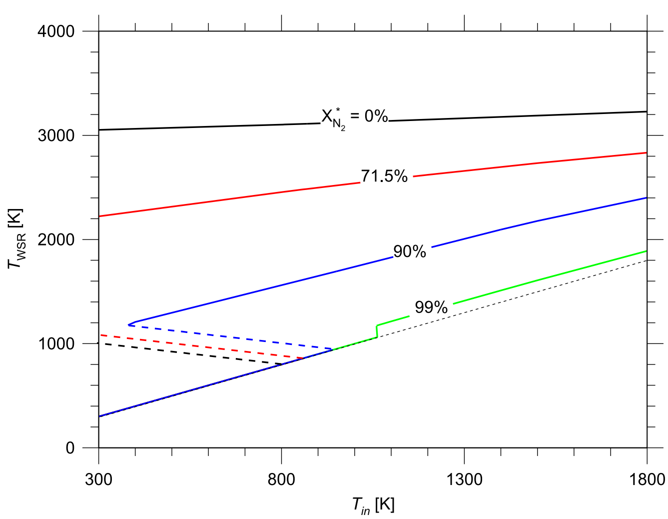

Fig. 5. WSR working temperatures (T_{WSR}) versus the inlet mixture temperature (T_{in}) with τ = 1.0 s for three different stoichiometric mixture compositions of $CH_4/O_2/N_2$, i.e., 6.7% O_2 + 3.3% CH_4 + 90% N_2, 19% O_2 + 9.5% CH_4 + 71.5% N_2, 66.7% O_2 + 33.3% CH_4 and 0.67% O_2 + 0.33% CH_4 + 99% N_2.

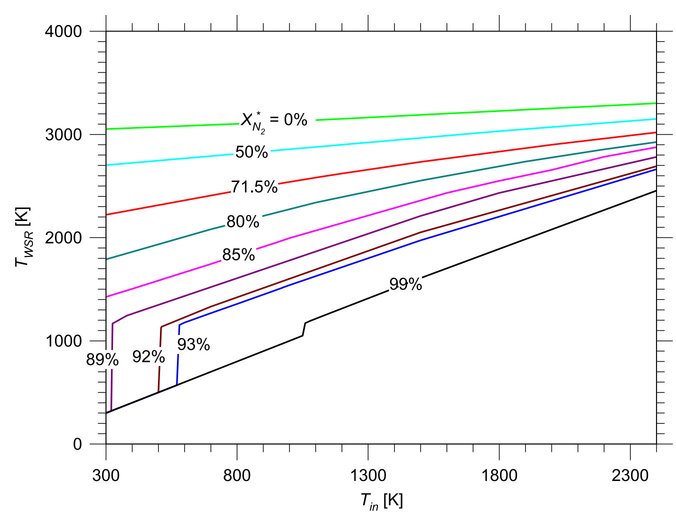

Fig. 6. WSR working temperatures (T_{WSR}) at the upper steady state as a function of the inlet temperature (T_{in}) for stoichiometric $CH_4/O_2/N_2$ mixture.

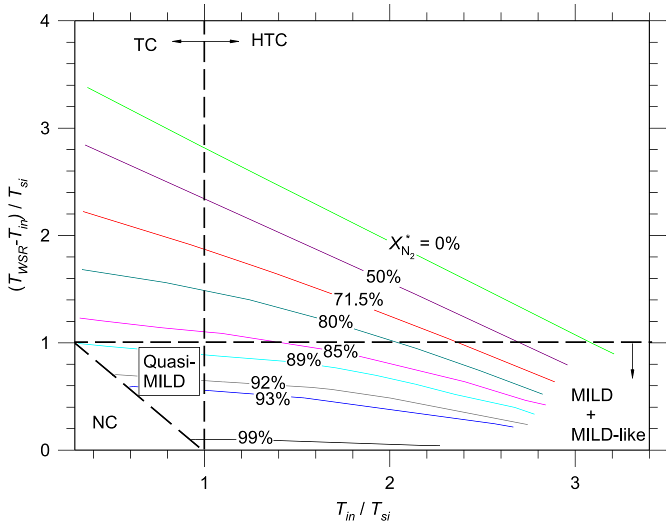

Fig. 7. WSR temperature increment in the upper steady state ($\Delta T = T_{WSR} - T_{in}$) versus the inlet temperature (T_{in}) for the stoichiometric $CH_4/O_2/N_2$ mixture. On the map, NC = no combustion; TC = traditional combustion; HTC = high temperature combustion; MILD = moderate or intense low-oxygen dilution.

$X^*_{N_2}$ = 99% or higher. This is also consistent with the previous observations for the low-oxygen combustion under the WSR [27] or the counter-flow diffusion conditions [28].

5. Classification of WSR combustion

Fig. 6 plots T_{WSR} at the upper steady state against T_{in} for the stoichiometric CH_4/O_2 mixture with $X^*_{N_2}$ ranging from 0% to 99%. Obviously, T_{WSR} decreases as $X^*_{N_2}$ is increased at a fixed T_{in}. This is because, at a higher $X^*_{N_2}$, the amount of the inlet reactants (CH_4/O_2) is less and thus less heat per unit the mixture is released, which consequently leads to a lower T_{WSR}. For each mixture composition, T_{WSR} increase monotonically with T_{in}. The reason is that the reactants initially carry more enthalpy at a higher T_{in}. Similar observations were also reported in refs. 1 and 16, but their discussions were all limited for $X^*_{N_2} \geq 71.5\%$. The T_{in}–T_{WSR} map can be easily transformed to a T_{in}–ΔT one, where ΔT is the working temperature increment, i.e., $\Delta T = T_{WSR} - T_{in}$. Since T_{si} varies with the $CH_4/O_2/N_2$ composition, the abscissa and ordinate of the T_{in}–ΔT plot are normalized using T_{si}.

Table 1
The classification of different regimes for $CH_4/N_2/O_2$ combustion in a WSR.

Combustion regime	Inlet conditions	Working conditions
Traditional combustion (TC)	$T_{in} < T_{si}$	$\Delta T > T_{si}$
High temperature combustion (HTC)	$T_{in} > T_{si}$	$\Delta T > T_{si}$
Flameless combustion (FLC)		
Quasi-MILD combustion	$T_{in} < T_{si}$	$\Delta T < T_{si}$
MILD + MILD-like combustion	$T_{in} > T_{si}$	$\Delta T < T_{si}$

As shown in Fig. 7, for a fixed T_{in}, ΔT decreases rapidly with increasing $X^*_{N_2}$ due to the reduction of T_{WSR}. More importantly, for any mixture composition, ΔT decreases with T_{in}, which can be explained here. The increase of T_{in} leads to a higher WSR working temperature, which is more beneficial to the dissociation of CO_2 and H_2O [18]. Evidently, a check of the outlet product composition reveals that an increase in T_{in} yields more unburnt combustible gases such as CO and H_2, see Fig. 8. In other words, as T_{in} is increased, less complete combustion takes place in the reactor and thus less reaction heat is released over the same residence time, hence reducing ΔT. In addition, the heat capacities of flue gases (e.g., CO_2, O_2, N_2, and H_2O) are expected to increase with temperature [18], and so for higher T_{in}, the same heat enables the flue gases to have a lower temperature rise. To summerize, both effects of the above chemical and physical factors due to increasing T_{in} result in the reduction of ΔT.

Following the method used by Cavaliere and de Joannon [1] for the WSR combustion, a vertical line at $T_{in}/T_{si} = 1$ and a horizontal line at $\Delta T/T_{si} = 1$ are drawn to divide the map into several regions, see Fig. 7. That is, the WSR combustion can be classified as the following four regimes, i.e., no combustion (NC), traditional combustion (TC), high temperature combustion (HTC), and flameless combustion (FLC), where FLC comprises the MILD, or MILD-like, and Quasi-MILD sub-regimes. The criterion for the various combustion regimes is summarized in Table 1.

In the NC region, T_{in} is less than T_{ex} and the reactants are so diluted that the released heat by the reaction cannot sustain the oxidation process. Hence, the combustion is extinct. The TC regime is located in the upper left of the map, where T_{in} is low and the working temperature increment is high, reflecting the typical

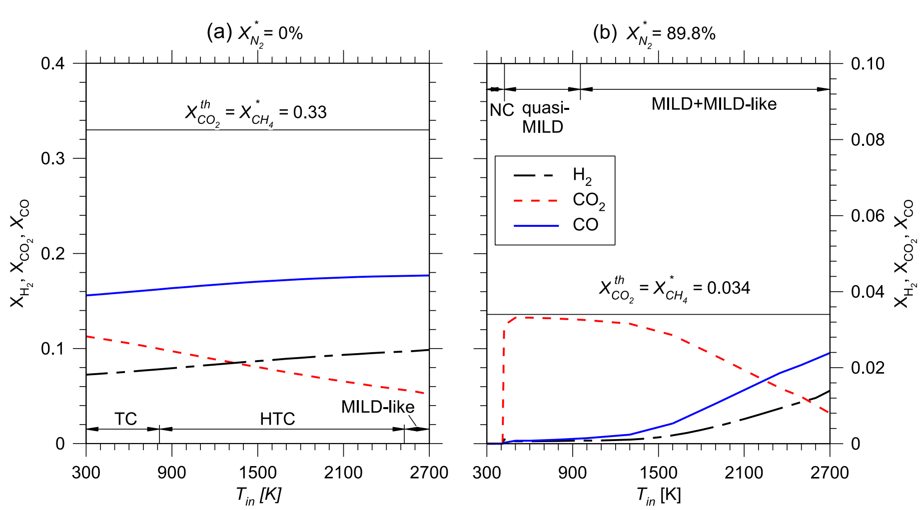

Fig. 8. Outlet product concentrations X_{H_2}, X_{CO_2} and X_{CO} versus the inlet temperature (T_{in}) for two stoichiometric $CH_4/O_2/N_2$ mixture compositions: (a) 66.7% O_2 + 33.3% CH_4 and (b) 6.7% O_2 + 3.3% CH_4 + 90% N_2. On the map, $X^{th}_{CO_2}$ is the theoretical CO_2 concentration of the flue gases; NC = no combustion; TC = traditional combustion; HTC = high temperature combustion; MILD = moderate or intense low-oxygen dilution.

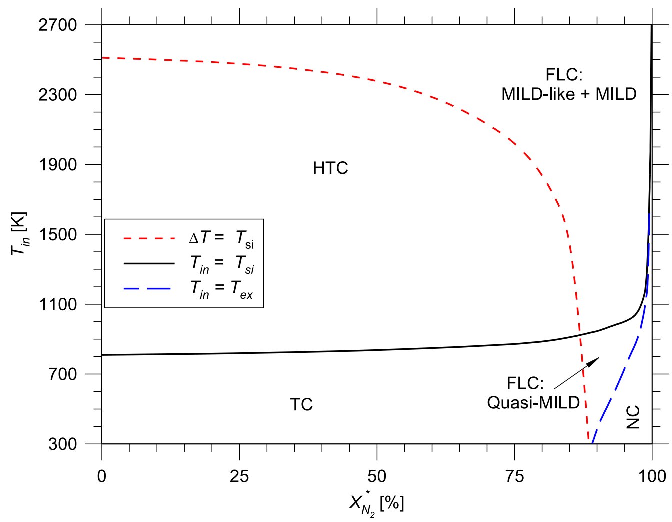

Fig. 9. Classification of the premixed stoichiometric $CH_4/O_2/N_2$ combustion in a WSR. On the map, T_{si} and T_{ex} are the self-ignition and extinction temperatures while $\Delta T = T_{WSR} - T_{in}$. NC = no combustion; TC = traditional combustion; HTC = high temperature combustion; MILD = moderate or intense low-oxygen dilution.

normal flames. As T_{in} is increased, the combustion state is transformed to the HTC regime where the combustion features differ from those of the TC. The lower region of the map belongs to the FLC because the temperature rise is sufficiently small at $\Delta T < T_{si}$ so that the flame might be invisible. More specifically, on the right of the FLC regime is the MILD or MILD-like combustion, where the high T_{in} of the reactants promotes and sustains the reaction process with a temperature rise smaller than T_{si}, i.e., $T_{in} > T_{si}$ and $\Delta T < T_{si}$. On the left, a triangular area represents a transitional region from the NC to the TC, HTC and MILD or MILD-like combustion. This transitional zone is featured by $T_{in} < T_{si}$ and $\Delta T < T_{si}$. In this zone, although T_{in} is not high enough to spontaneously ignite the reactants or cause fast combustion reactions, the accumulation of the input heat energy carried by the preheated initial mixture and the heat released from exothermic reactions can sustain slow or '*mild*' combustion. Based on these characteristics, this transitional zone is named as 'Quasi-MILD' in the FLC regime. Note that similar observations to the transitional zone were also reported in Refs. [12,13,15].

Fig. 8 shows the concentrations of the outlet unburnt combustible gases (CO and H_2) versus the inlet temperature T_{in}. Quite obviously, as T_{in} is increased, the emissions of CO and H_2 grow steadily. That is, at a higher T_{in}, the conversion from CH_4 to CO_2 becomes less complete. Fig. 8(a) shows that the CO_2 emission (X_{CO_2}) is far less than the theoretical one ($X^{th}_{CO_2}$) for the non-dilution case. This indicates that the conversion rate from CH_4 to CO_2 is very small no matter at which regime the combustion occurs. In contrast, for the diluted case (Fig. 8(b)), the initial CH_4 is nearly completely oxidized into CO_2, i.e., $X_{CO_2} \approx X^{th}_{CO_2} = X^*_{CH_4}$ when $T_{in} < 1300$ K, which means the high conversion rate from CH_4 to CO_2 under quasi-MILD or MILD combustion regimes. However, when $T_{in} > 1300$ K, X_{CO_2} begins to decrease with further increasing T_{in}. Hence, the conversion from CH_4 to CO_2 becomes less complete at high inlet temperatures even under MILD or MILD-like conditions. From this, although MILD and MILD-like combustion can well satisfy the mathematical definition [1] by increasing T_{in} for any reactant composition, the occurrence of these regimes, especially for non-diluted and enriched cases, is achieved at the expense of reduction in conversion rate from CH_4 to CO_2. Therefore, when referred to the mathematical definition [1] of MILD combustion, the conversion rate from CH_4 to CO_2 should also be considered in the indentification of MILD combustion. Besides, considering the adiabatic conditions of the present WSR calculations, the reaction heat released cannot be transferred outside via the reactor wall. However, it is important to note that this situation will change if the WSR is replaced by a practical combustor such as a heating furnace. In the latter, the reaction heat is continuously transferred away and hence the reacting temperature drops along the reaction process, finally terminating the dissociation of CO_2 and H_2O. Therefore, the fuel will surely be burnt out for $\phi < 1$ with sufficiently long reacting or residence time.

With the aid of T_{in}-ΔT map, various combustion regimes can be identified under different combustor configurations, as shown in the numerous existing publications [1,11–14]. However, the shortcoming of using $T_{in}-\Delta T$ map is obvious that one cannot determine the combustion regime a priori because the operative conditions are given by T_{in}, reactant concentrations (X^*_i), and φ, rather than ΔT. Consequently, the $T_{in}-\Delta T$ map is not available to directly determine which regime the combustion will be evolved under given conditions (T_{in}, X^*_i, and φ). To address this issue, we transform the $T_{in}-\Delta T$ map of Fig. 7 into a $T_{in}-X^*_{N_2}$ map, shown in Fig. 9. On the map, the four aforementioned combustion regimes are clearly indentified using the three lines, i.e., $T_{in} = T_{ex}$, $T_{in} = T_{si}$ and $\Delta T = T_{si}$. Fig. 9 demonstrates that the mathematical definition of MILD combustion [1] can be well satisfied as long as T_{in} is sufficiently high. In other words, the MILD and MILD-like combustion as a whole can occur for all cases even without reactant dilution. For instance, MILD or MILD-like combustion can occur in the cases with

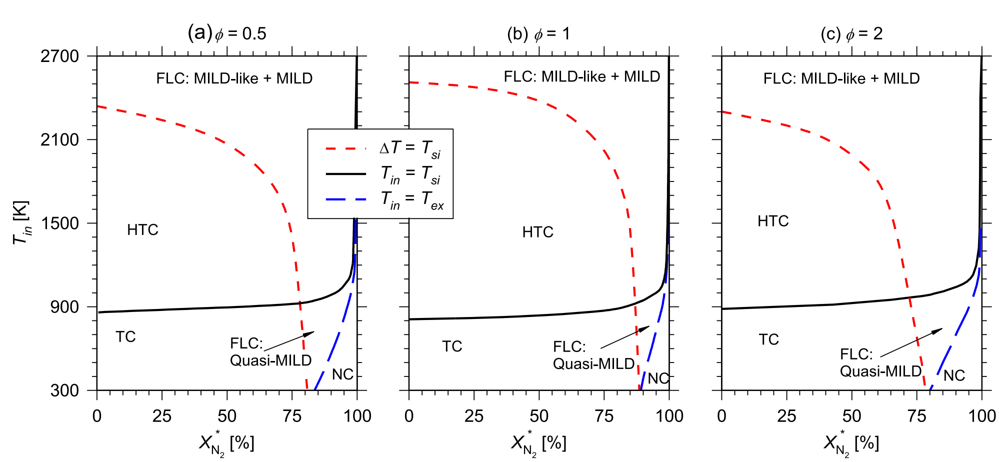

Fig. 10. Classifications of the premixed $CH_4/O_2/N_2$ WSR combustion at (a) $\varphi = 0.5$, (b) $\varphi = 1.0$, and (c) $\varphi = 2.0$. On the map, NC = no combustion; TC = traditional combustion; HTC = high temperature combustion; MILD = moderate or intense low-oxygen dilution.

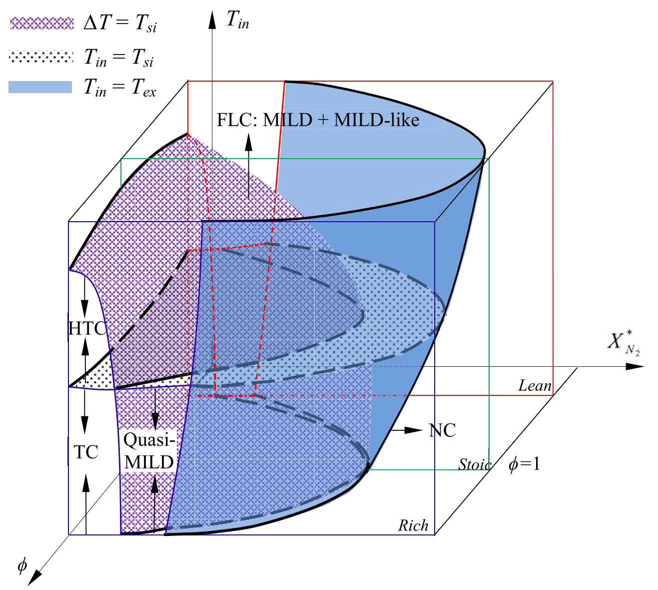

Fig. 11. Schematic 3D diagram showing the combustion regimes expressed in terms of φ, T_{in} and $X^*_{N_2}$. On the diagram, NC = no combustion; TC = traditional combustion; HTC = high temperature combustion; MILD = moderate or intense low-oxygen dilution.

$T_{in} > 2520$ K and $X^*_{N_2} = 0\%$ and those with $T_{in} > 945$ K and $X^*_{N_2} = 90\%$. Moreover, through Fig. 9, one can directly determine the final combustion regime from any given operative conditions (T_{in}, X_i^*) while it is hard, at least inconvenient, to make such estimations from the T_{in}–ΔT map. On the other hand, the overall combustion regime classification depends little on the combustor configurations, because the same regimes can be also classified in the previous diffusion systems [12,13,15].

In fact, the local equivalence ratio inside a furnace cannot be always unity. Accordingly, to emulate the combustion inside a practical furnace, the effect of φ is also examined. Fig. 10 indicates the classifications of different combustion regimes at $\varphi = 0.5$ (fuel lean), 1.0 (stoichiometric) and 2.0 (fuel rich). As expected, for the three values of φ, the three maps are overall similar, but the locations and sizes of the regimes change. Apparently, the line of $T_{in} = T_{si}$ is lower, whereas that of $\Delta T = T_{si}$ is higher, for the stoichiometric mixture than for the other two cases. This is because the fuel can be more easily ignited and burned out under the stoichiometric condition. Also, under the same dilution level, T_{WSR} for $\varphi = 1.0$ should be higher than those of $\varphi = 0.5$ and $\varphi = 2.0$, so that a higher T_{in} is required to satisfy the MILD combustion condition $\Delta T = T_{WSR} - T_{in} < T_{si}$.

Based on the results of Fig. 10 and those for other values of φ, the classification for the $CH_4/O_2/N_2$ combustion can be illustrated schematically in a three-dimensional plot ($T_{in} - \varphi - X^*_{N_2}$), see Fig. 11. It is demonstrated that the extinction limit is extended to higher $X^*_{N_2}$ as T_{in} is increased and/or $\varphi \rightarrow 1$. The $T_{in} = T_{ex}$ plane represents the critical operative conditions beyond which no combustion occurs. The reaction region is then divided into two regions by the $T_{in} = T_{si}$ plane, below which the reactant self-ignition cannot take place. The addition plane of the $\Delta T = T_{si}$ enables the WSR combustion to be subdivided into five regimes, i.e., no combustion (NC), traditional combustion (TC), high temperature combustion (HTC), Quasi-MILD combustion, MILD or MILD-like combustion. Here, the MILD or MILD-like and Quasi-MILD combustion constitute the flameless combustion (FLC). From Fig. 11, one can easily identify the combustion regime for any given conditions (temperature, reactants equivalence ratio, and dilution ratio). Moreover, Medwell and Dally [29] found that the fuel type does not have a significant effect on the combustion reaction characteristics. Therefore, when referred to other fuels, the combustion regimes shown in Fig. 11 should also apply.

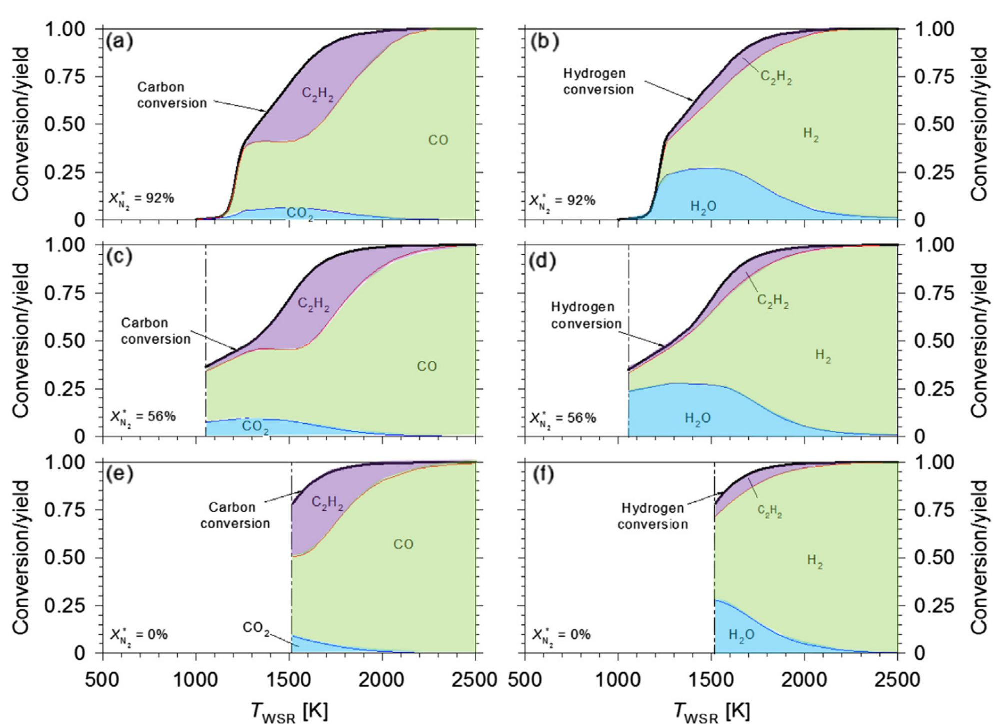

Fig. 12. Conversions of the initial C and H to CO, CO_2, C_2H_2, H_2O and H_2 as functions of T_{WSR} at $\tau = 1.0$ s and $\varphi = 4.0$. Solid black lines represent the C and H conversions whereas the marked areas denote the contributions of C and H conversions to the productions of CO, CO_2, C_2, H_2O and H_2 at three different N_2 dilution levels.

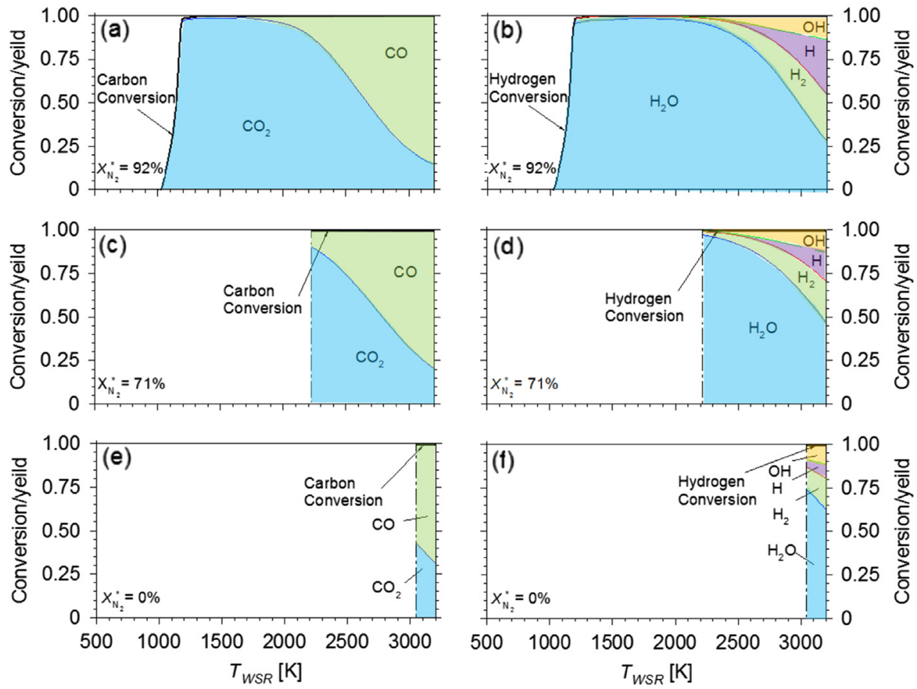

Fig. 13. Conversions of the initial C and H to CO, CO_2, H_2, H_2O, H and OH as functions of T_{WSR} at $\varphi = 1.0$ and $\tau = 1.0$ s. The three different N_2 dilution levels are indicated on the plots.

6. Characteristics of WSR combustion

6.1. Overall mechanism of CH_4 oxidation

Following the above discussion, it is aware that the transition between the combustion regimes and different T_{WSR} can be achieved by varying the inlet reactant conditions, i.e., φ, T_{in} and $X^*_{N_2}$. One would then ask whether the products composition remain the same under different combustion regimes. It is hence worthy to investigate the effects of φ, T_{in} and $X^*_{N_2}$ on the overall reaction mechanisms of CH_4 combustion when varying combustion regimes.

Fig. 12 presents the contributions of the initial carbon (C) and hydrogen (H) atom to the productions of CO, CO_2, C_2H_2, H_2O and H_2 as functions of T_{WSR} at $\tau = 1.0$ s and $\varphi = 4.0$. As claimed in Ref. [16], C_2H_2 is the most important one of the C_2 compounds (C_2H_6, C_2H_5, C_2H_4, C_2H_3, and C_2H_2) formed through recombination. Thus, only

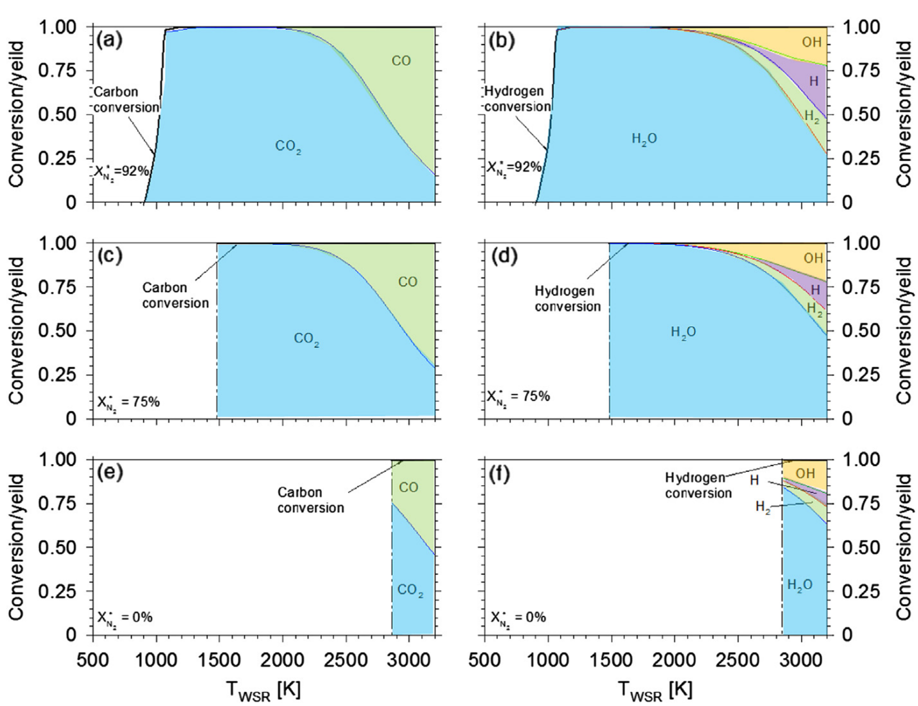

Fig. 14. Conversions of the initial C and H to CO, CO_2, H_2, H_2O, H and OH as functions of T_{WSR} at $\varphi = 0.5$ and $\tau = 1.0$ s. The three different N_2 dilution levels are indicated on the plots.

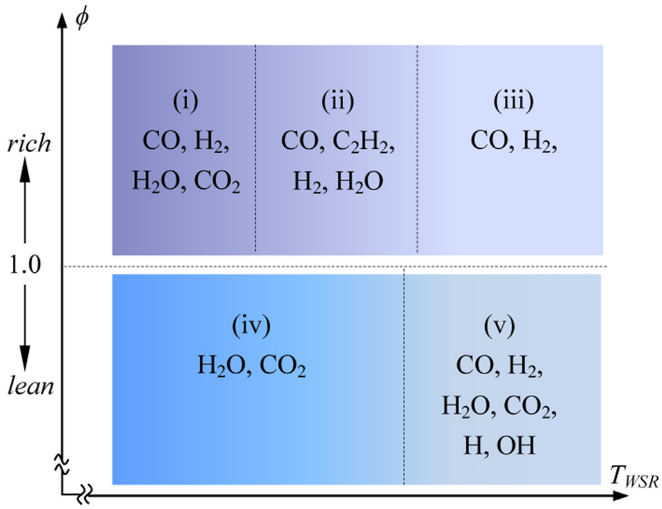

Fig. 15. Products of CH_4 oxidation dependence on φ and T_{WSR}.

C_2H_2 are presented here. The solid lines on the plots represent the ratios between the converted and inlet moles of atomic C (left) and H (right). The colored areas denote the C and H yields of the main produced species (C → CO, CO_2, C_2H_2 and H → H_2O, H_2, C_2H_2). In addition, the curves of Fig. 12(a) and (b) start at T_{WSR} = 1242 K, where T_{ex} = 1050 K is located for φ = 4.0 and $X^*_{N_2}$ = 92%. In contrast, the starting points of the curves in Fig. 12(c–f) are T_{WSR} = 1052 K and 1520 K at T_{in} = 300 K for $X^*_{N_2}$ = 56% and 0%.

For T_{WSR} < 1300 K, Fig. 12(a–d), CO, H_2, and H_2O are the main products with a small amount of CO_2 and almost no C_2H_2. For 1300K ≤ T_{WSR} ≤ 2000 K, Fig. 12 demonstrates that the concentrations of CO and H_2 increase rapidly while those of CO_2 and H_2O decrease and C_2H_2 becomes important. This is because the recombination channel, through which CH_4 can be partly recombined to the $C_{(2)}$ compound, becomes more important than the oxidation channel in this range of T_{WSR} [16]. Then, a further increase of T_{WSR} leads all the C and H to be conversed to CO and H_2, and hence CO_2, H_2O and C_2H_2 further decrease to zero. The present results, Fig. 12(a), are nearly the same as reported in Ref. [16]. The authors stated that, for the $CH_4/O_2/N_2$ mixture at φ = 4 and $X^*_{N_2}$ = 85%, the CH_4 reaction mechanisms vary greatly with T_{WSR}. Based on Fig. 12, the most representative overall mechanisms for the CH_4 oxidation can be expressed as

(i) for T_{WSR} < 1300 K: $CH_4 + O_2 \rightarrow CO + H_2 + H_2O$;
(ii) for 1300 < T_{WSR} < 2000 K: $CH_4 + O_2 \rightarrow CO + H_2O + H_2 + C_2H_2$;
(iii) for T_{WSR} > 2000 K: $CH_4 + O_2 \rightarrow CO + H_2$.

Figs. 13 and 14 show the ratios of C and H yielding the products (i.e., CO, CO_2, H_2, H_2O, H and OH) for φ = 1.0 and 0.5. In these figures, the solid lines denote the ratios between the converted and inlet moles of atomic C (left) and H (right). For $X^*_{N_2}$ = 92%, the conversion curves start at T_{WSR} ≈ 500 K and 400 K for φ = 1.0 and 0.5. For other cases, CH_4 is completely consumed and hence the H and C conversion ratios are all equal to 1 (see Figs. 13 (c–f) and 14 (c–f)). The colored areas represent the ratios of C, H atom conversion to the main products (C → CO, CO_2 and H → H_2O, H_2, H, OH). In addition, very little C_2 compounds are produced for these cases, and hence they are not given on the plots. Similar as that for φ = 4.0, the yielding ratios of C and H to the products also appear to be a function of T_{WSR} for the two values of φ at any diluting level. CO_2 and H_2O are found to be the main products for T_{WSR} < 2000 K, as shown in Figs. 13(a–d) and 14(a–d). For T_{WSR} > 2000 K, CO, H_2, H, and OH become important, while the ratios of C and H converted to CO_2 and H_2O decrease. In these cases, the global mechanisms of the CH_4 oxidation can be proposed as:

(iv) for T_{WSR} < 2000 K: $CH_4 + O_2 \rightarrow CO_2 + H_2O$;
(v) for T_{WSR} > 2000 K: $CH_4 + O_2 \rightarrow CO + CO_2 + H_2O + H_2 + H + OH$.

Following the overall reactions given in (i) ~ (v), Fig. 15 indicates the impacts of T_{WSR} and ϕ on the products of CH_4 oxidation. For fuel-rich conditions, the increase of T_{WSR} leads to three compositions of the products: (i) CO + H_2 + H_2O + CO_2, (ii) CO + C_2H_2 + H_2 + H_2O and (iii) CO + H_2. In contrast, no $C_{(2)}$ compound can be produced in the stoichiometric or fuel-lean conditions. The increase of T_{WSR} hence only results in the two compositions of the products: (iv) CO_2 + H_2O and (v) CO + H_2 + H_2O + CO_2 + OH + H. Moreover, according to Fig. 11, the combustion regime transition can be achieved by changing T_{in}. Thus, the WSR combustions for the cases of Figs. 12–14 have all experienced the regime change. Of interest, the fuel conversion and its corresponding contributions to the products appear to be independent of any combustion regime. Hence, the combustion regime has little influence on the overall CH_4 reaction paths. In other words, the global kinetic mechanism for CH_4 oxidation should depend mainly on T_{WSR} and φ rather than the initial dilution level and the combustion regime.

6.2. Elementary reactions of oxidizing CH_4

Based on the WSR calculations, the elementary chemical pathways of the conversion from CH_4 to CO_2 for cases 1–6 (Table 2) are displayed in Fig. 16. On the diagrams, arrows represent elementary reactions with the primary reactant species at the tail and the primary product species at the head. Other reactant species are shown aside of the arrows and the corresponding reactions (marked in accordance with GRI-Mech 3.0) are also indicated. The arrow width gives a visual indication of the relative importance of a particular reaction, where the numbers in parentheses quantitatively show the reaction rates. For instance, 2.4–7 means 2.4×10^{-7} (gmol/cm^3 s). In the diagrams, unimportant reactions are ignored. In other words, only those pathways with reaction rates higher than 1×10^{-8} gmol/cm^3 s and 1×10^{-9} gmol/cm^3 s for cases 1–5 and case 6, are shown.

The main pathways of CH_4/O_2 mixture reactions at different operative conditions can be summarized briefly as follows:

i) For Cases 1–3, 6:

As shown in Fig. 16(a~c, f), CH_4 converses mainly through the central path to CO_2, with several side paths originating from the methyl (CH_3) radical. For the central path, CH_4 molecule firstly undergoes H abstraction due to the attack by OH, O, and H radicals and produces the methyl radical (CH_3). The CH_3 then combines with an oxygen atom to form formaldehyde (CH_2O), which, in turn, is attacked by OH and H radicals to produce the formyl radical

Table 2
Operative conditions for CH_4 reaction analysis under different combustion regimes.

Case	Mixture composition	T_{in}	T_{WSR}	Combustion regime
1	33% CH_4 + 67% O_2	700 K	3090 K	TC
2	33% CH_4 + 67% O_2	1500 K	3189 K	HTC
3	33% CH_4 + 67% O_2	2700 K	3338 K	MILD-like
4	92% N_2 + 2.7% CH_4 + 5.3% O_2	700 K	1312 K	Quasi-MILD
5	92% N_2 + 2.7% CH_4 + 5.3% O_2	1500 K	2052 K	MILD
6	92% N_2 + 2.7% CH_4 + 5.3% O_2	2700 K	2867 K	MILD

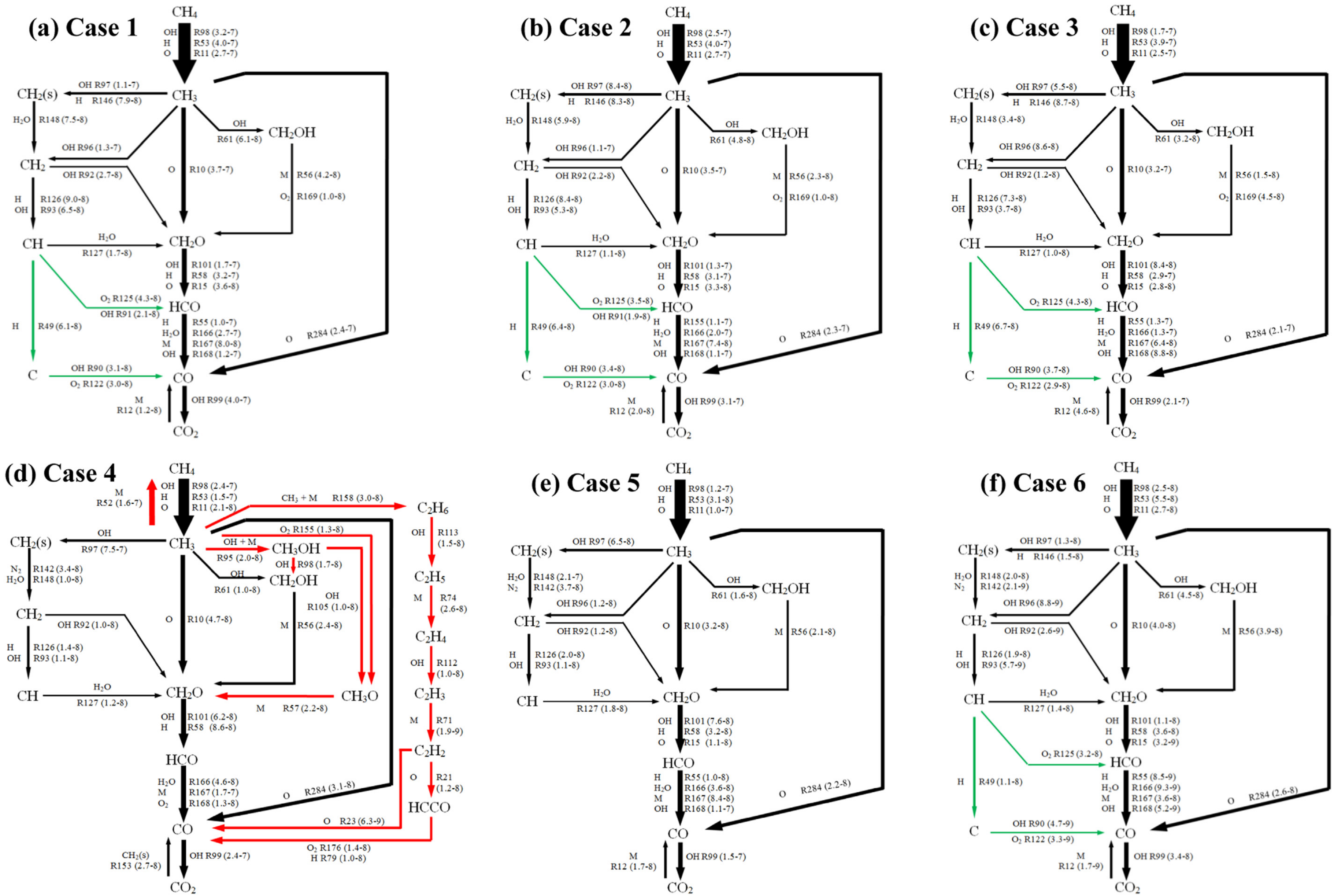

Fig. 16. Reaction pathways for the non-diluted (a~c: cases 1–3) and diluted (d~f: cases 4~6) CH_4 combustion for $\tau = 1.0$ s in a WSR, under different combustion regimes, i.e., case 1: Traditional combustion (TC), case 2: high temperature combustion (HTC), case 3: MILD-like combustion, case 4: Quasi-MILD combustion and case 5, 6: MILD or MILD-like combustion. Note that, the parenthetical numbers denote the reaction rates, e.g., 2.4–7 meaning 2.4×10^{-7} (gmol/cm^3 s).

(HCO). Next, the HCO reacts with H_2O and O_2 to form CO. Finally, CO is converted to CO_2, mainly reacting with OH.

For the side paths, all start from CH_3. On the left, CH_3 reacts with OH radical to form methylene radical in two possible electronic configurations (CH_2(s) and CH_2). CH_2(s) reacts with H_2O and N_2 and is translated to CH_2, which forms CH_2O, HCO and then CO; note that CH_2(s) only reacts with H_2O in non-diluted cases because the initial reactant mixture does not contain any N_2. Or CH_2 is dehydrogenated to form CH and C, which is then transformed to HCO and CO. Moreover, there are two different paths on the right side: i.e., CH_3 is either converted to CH_2OH and then forms CH_2O, HCO and CO or is directly transformed to CO and then CO_2.

ii) For Case 5:

It differs only slightly from cases 1–3 and 6. The two-dehydrogenation reactions $CH_2 \rightarrow CH \rightarrow C \rightarrow CO$ and $CH_2 \rightarrow CH \rightarrow HCO \rightarrow CO$ [green arrows in Fig. 16 (a~c, f)] are found to disappear.

iii) For Case 4:

Apart from all pathways shown in Fig. 16(a~c and e~f), those paths that are unimportant or even absent for cases 1–3, 5 and 6 become prominent for case 4. As demonstrated in Fig. 16(d), red arrows show the new important pathways at relative low reacting temperature and complement the diagram for the high temperature cases. In the path map, several interesting pathways appear. Firstly, CH_3 is found to strongly react backward to CH_4. Then, a new route from CH_3 to CH_2O appears, along which CH_3 reacts with OH to produce methanol (CH_3OH) and CH_3O. Importantly, a recombination route is observed to form $C_{(2)}$ hydrocarbons, which is a common feature of the low-temperature oxidations. In the path of recombination channel, CH_3 radicals are recombined to form ethane (C_2H_6), which is ultimately converted to CO and CH_2 through a series of C_2H_x hydrocarbons.

CH_4 reaction pathways for cases 1–3 appear to be very similar although the combustion regime has been changed when T_{in} varies from 700 K to 2700 K. The reason behind is that the WSR working temperature T_{WSR} changes very little, i.e., from 3090 K to 3338 K, as T_{in} is increased. Therefore, according to ref. 18, the chemical pathways for the three cases all follow the high temperature reaction pattern. In contrast, for cases 5–6, the combustion regime changes from quasi-MILD to MILD when T_{in} varies from 700 K to 2700 K. Obviously, the CH_4 reaction pathways differ greatly. This should result from the fact that T_{WSR} increases significantly from 1312 K to 2867 K as T_{in} increases from 700 K to 2700 K. Consequently, the low temperature chemical pathway pattern for case 4 is changed to the high temperature one for case 6 [18]. It is also interesting to note that the CH_4 oxidation pathways are similar for cases 1–3 and f because $T_{WSR} \approx 3000$ K for all these cases. From the above discussion, although the investigated cases are under different combustion regimes, the reaction pathways are found to mainly depend on T_{WSR}. In other words, the reacting temperature has a significantly stronger influence on combustion pathways than does the combustion regime.

7. Conclusions

The present study has characterized and also classified the WSR combustion of $CH_4/O_2/N_2$ based on the kinetic calculations over wide ranges of the inlet mixture temperature (T_{in}), nitrogen concentration for dilution ($X^*_{N_2}$) and equivalence ratio (φ). The *S*-curve is utilized to identify the extinction and self-ignition temperatures (T_{ex} and T_{si}) of the $CH_4/O_2/N_2$ mixture, from which the mapping of the various combustion regimes is obtained. On the basis of the results presented in Sections 5 and 6, several conclusions are made below.

1. The T_{ex} and T_{si} can be changed by varying either the dilution degree or the residence time in the reactor or by both. As the dilution is increased and/or the residence time is decreased, both T_{ex} and T_{si} increase, but their difference narrows rapidly.
2. A three-dimensional T_{in}–$X^*_{N_2}$–φ plot is produced. From it, the combustion regime at any given operative condition can be easily identified, i.e., the traditional combustion (TC), high temperature combustion (HTC), and flameless combustion (FLC), where FLC may be further divided into the three subzones: MILD, MILD-like and quasi-MILD.
3. The classification of the combustion regime appears to be generic and depend little on the combustor configuration because similar observations can be made from the present WSR combustion and diffusion flames under different configurations [12,13,15].
4. Both the overall mechanism and elementary chemical pathways of CH_4 oxidation depend mainly on T_{WSR} and φ, and weakly on the combustion regime. This conclusion derives from analyzing the fuel conversion to the composition of the WSR products under various initial conditions.

Acknowledgments

The authors gratefully acknowledge the support of the Special Research Fund for the Doctoral Program of Higher Education of China (Grant No. 20110001130014), Natural Science Foundation of China (Grant No. 51276002) and the Centre for Global New Energy Strategy Studies of Peking University.

References

[1] Cavaliere A, de Joannon M. MILD combustion. Prog Energy Combust Sci 2004;30(4):329–66.
[2] Wünning JA, Wünning JG. Flameless oxidation to reduce thermal NO-formation. Prog Energy Combust Sci 1997;23(1):81–94.
[3] Katsuki M, Hasegawa T. The science and technology of combustion in highly preheated air. Proc Combust Inst 1998;27(2):3135–46.
[4] Tsuji H, Gupta AK, Hasegawa T, Katsuki K, Kishimoto K, Morita M. High temperature air combustion: from energy conservation to pollution reduction. United States, Florida, Boca Raton FL: CRC Press; 2003.
[5] Yu B, Kum S, Lee C, Lee S. Effects of exhaust gas recirculation on the thermal efficiency and combustion characteristics for premixed combustion system. Energy 2013;49:375–83.
[6] Mi J, Li P, Zheng C. Impact of injection conditions on flame characteristics from a parallel multi-jet burner. Energy 2011;36(11):6583–95.
[7] Gao X, Duan F, Lim S, Yip M. NO_x formation in hydrogen–methane turbulent diffusion flame under the moderate or intense low-oxygen dilution conditions. Energy 2013;59:559–69.
[8] Plessing T, Peters N, Wünning JG. Laser optical investigation of highly preheated combustion with strong exhaust gas recirculation. Proc Combust Inst 1998;27(2):3197–204.
[9] Mi J, Wang F, Li P, Dally BB. Modified vitiation in a moderate or intense low-oxygen dilution (MILD) combustion furnace. Energy Fuels 2012;26(1):265–77.
[10] Lille S, Blasiak W, Jewartowski M. Experimental study of the fuel jet combustion in high temperature and low oxygen content exhaust gases. Energy 2005;30(2–4):373–84.
[11] de Joannon M, Sabia P, Sorrentino G, Cavaliere A. Numerical study of MILD combustion in hot diluted diffusion ignition (HDDI) regime. Proc Combust Inst 2009;32(2):3147–54.
[12] Chen S, Mi J, Liu Z, Zheng C. First and second thermodynamic-law analyses of hydrogen-air counter-flow diffusion combustion in various combustion modes. Int J Hydrogen Energy 2012;37(6):5234–45.
[13] de Joannon M, Sorrentino G, Cavaliere A. MILD combustion in diffusion-controlled regimes of hot diluted fuel. Combust Flame 2012;159(5):1832–9.
[14] de Joannon M, Sabia P, Cozzolino G, Sorrentino G, Cavaliere A. Pyrolitic and oxidative structures in hot oxidant diluted oxidant (HODO) MILD combustion. Combust Sci Tec 2012;184(7–8):1207–18.

[15] Wang F, Mi J, Li P. Combustion regimes of a jet diffusion flame in hot coflow. Energy Fuels 2013;27(6):3488–98.
[16] de Joannon M, Saponaro A, Cavaliere A. Zero-dimensional analysis of diluted oxidation of methane in rich conditions. Proc Combust Inst 2000;28(2):1639–46.
[17] de Joannon M, Cavaliere A, Faravelli T, Ranzi E, Sabia P, Tregrossi A. Analysis of process parameters for steady operations in methane mild combustion technology. Proc Combust Inst 2005;30(2):2605–12.
[18] Turns SR. An introduction to combustion: concepts and applications. New York: McGraw Hill Higher Education; 1996.
[19] Dally BB, Karpetis AN, Barlow RS. Structure of turbulent non-premixed jet flames in a diluted hot coflow. Proc Combust Inst 2002;29(1):1147–54.
[20] Kee R, Rupley FM, Millerm JA, Coltrin JA, Grcar JF, Meeks E, et al. CHEMKIN collection, release 4.1. San Diego CA: Reaction Design Inc.; 2010.
[21] Smith GP, Golden DM, Frenklach M, Moriarty NW, Eiteneer B, Goldenberg M, et al. Available via the Internet at: www.me.berkeley.edu/gri-mech/.
[22] Wang F, Mi J, Li P, Zheng C. Diffusion flame of a CH_4/H_2 jet in hot low-oxygen coflow. Int J Hydrogen Energy 2011;36(15):9267–77.
[23] Wang F, Li P, Mei Z, Mi J. Auto- and forced-ignition temperatures of diffusion flames obtained through the steady RANS modeling. Energy Fuels 2014;28(1):666–77.
[24] Oh Jeongseog, Noh Dongsoon. Laminar burning velocity of oxy-methane flames in atmospheric condition. Energy 2012;45(1):669–75.
[25] Steven Z, Joseph Z. Chemical kinetics of NO_x production in a well stirred reactor. AIAA J 1994;3828:649–53.
[26] Law CK. Combustion physics. United Kingdom, Oxford: Cambridge University Press; 2006.
[27] Oberlack M, Arlitt R, Peters N. On stochastic Damköhler number variations in a homogeneous flow reactor. Combust Theory Model 2000;4(4):495–509.
[28] Ihme M, Zhang J, He G, Dally B. Large-eddy simulation of a jet-in-hot-coflow burner operating in the oxygen-diluted combustion regime. Flow Turbul Combust 2012;89(3):449–64.
[29] Medwell PR, Dally BB. Effect of fuel composition on jet flames in a heated and diluted oxidant stream. Combust Flame 2012;159(10):3138–45.